

---

# **Evaluation of VSAERO in Prediction of Aerodynamic Characteristics of Helicopter Hub Fairings**

---

Alexander Louie, Ames Research Center, Moffett Field, California

February 1989



National Aeronautics and  
Space Administration

**Ames Research Center**  
Moffett Field, California 94035

## SYMBOLS

$C_D$	Drag coefficient nondimensionalized by planform area and $q_\infty$
$C_L$	Lift coefficient nondimensionalized by planform area and $q_\infty$
$C_P$	Pressure coefficient
$D$	Hub-fairing diameter
$\mathbf{F}$	Force vector on wake panel
$H$	Shape factor
$\Delta H$	Change in total pressure
$\mathbf{n}$	Normal unit vector to body surface
$q_\infty$	Free-stream dynamic pressure
$s$	Distance along a surface
$S$	Surface of the configuration
$S_\infty$	Reference surface which encloses the complete flow field at infinity
$\mathbf{V}$	Velocity vector
$V$	Magnitude of $\mathbf{V}$
$W$	surface
$\alpha$	Angle of attack of hub fairings (degrees)
$\gamma$	Vorticity vector density
$\Gamma$	Circulation vector
$\delta^*$	Boundary-layer displacement thickness
$\theta$	Boundary-layer momentum thickness
$\rho$	Air density
$\Phi$	Total velocity potential

### Subscripts

<i>ave</i>	Average value
<i>e</i>	Outer edge of boundary layer
<i>i</i>	Inner region (inside body)
<i>in</i>	Conditions inside the wake region
<i>N</i>	Normal component
<i>p</i>	Conditions at point P in the flow field
<i>out</i>	Conditions outside the wake region
<i>O</i>	Outer region
<i>sep</i>	Conditions at separation
<i>U, L</i>	Upper and lower surface, respectively

PRECEDING PAGE BLANK NOT FILMED

# SUMMARY

A low-order panel code, VSAERO, was used to predict the aerodynamic characteristics of helicopter hub fairings. Since the simulation of this kind of bluff body by VSAERO was not documented before, the VSAERO solutions were correlated with experimental data to establish their validity. The validation process revealed that simulation of the aerodynamic environment around a hub fairing was sensitive to several modeling parameters. Some of these parameters are body and wake panels arrangement, streamwise and spanwise separation location, and the most prominent one — the wake modeling.

Three wake models were used: regular wake, separated wake, and jet model. The regular wake is a wake with negligible thickness (thin wake). It is represented by a single vortex sheet. The separated wake and the jet model in the present application are wakes with finite thickness (thick wake). They consist of a vortex sheet enclosing a region of low-energy flow. The results obtained with the regular wake were marginally acceptable for sharp-edged hub fairings. For all other cases under consideration, the jet model results correlated slightly better. The separated wake, which seemed to be the most appropriate model, caused the solution to diverge. While the regular wake was straight-forward to apply in simulations, the jet model was not. It requires the user to provide information about the doublet strength gradient on wake panels by guessing the efflux velocities at the wake shedding location. To obtain the correct doublet strength, these estimated velocities were matched to the calculated values. This involved an arduous and impracticable iterative process. In summary, VSAERO neither predicts accurately the aerodynamic characteristics of helicopter hub fairings nor was cost effective.

## 1 INTRODUCTION

Hub and shaft parasite drag comprises 20 to 50% of the total drag of a typical helicopter. Power requirements could be significantly reduced and/or performance could be improved if this component of drag is reduced (ref. 1). These incentives have stimulated much research effort involving experimental and analytical work (refs. 1 – 4). The Hub Drag Reduction Program at NASA Ames Research Center (ARC) was initiated to continue the study of drag associated with helicopter hubs. The program objectives are to understand more about the flow characteristics around the hub and shaft fairing and to develop drag reduction methods.

Two small-scale wind tunnel tests were conducted recently at ARC to investigate the drag mechanisms associated with flow around a nonrotating hub fairing. Stationary fairings were studied because previous research had shown that the effect of rotation was small when blade shanks were removed. The test results (refs. 5 and 6; Graham, D. R.; Sung, D. Y.; and Young, L. A.: A Small-Scale Investigation of Helicopter Hub and Pylon Fairing Drag Characteristics. To be published as NASA TM-101052) indicate that hub-fairing geometry, such as camber and surface curvature, could significantly influence the flow field over a large area of the helicopter, which in turn changes the overall drag. In addition to these findings, the tests also produced a data base to validate theoretical and empirical prediction methodologies.

As part of the analytical effort of the Hub Drag Reduction Program, the computer code VSAERO was used to predict the aerodynamic loads and flow characteristics of hub fairings in incompressible flow. These simulations were limited to isolated fairings, thus no interference effects from the sting support or the wind tunnel walls were included. The main objective was to optimize low-drag hub fairing designs.

The VSAERO results were correlated with test data obtained for isolated hub fairings mounted on a small sting support in the ARC 7- by 10-Foot Wind Tunnel (fig. 1). The support was designed to minimize the aerodynamic interference between the hub fairing and the sting. To establish the validity of VSAERO in predicting hub fairing

aerodynamics, five fairings were selected for correlation both quantitatively (measured aerodynamic loads) and qualitatively (flow visualization using laser sheet and oil flow techniques).

The VSAERO wake models which are essential in understanding the nature of the simulation are discussed in the report. Also presented are some peculiar problems associated with paneling of fairings, determination of separation location, and wake modeling. The results of the validation effort and the applicability of VSAERO in predicting aerodynamic characteristics of hub fairings are summarized.

## 2 VSAERO MODEL OF THE HUB FAIRINGS

VSAERO is a computer code designed for calculation of "the subsonic aerodynamic characteristics of arbitrary configurations having vortex separation and strong vortex-surface interaction (ref. 7)." The program formulation is based on a low-order, potential-flow-panel method with piecewise constant doublet and source singularities, coupled with integral boundary-layer methods. Nonlinear effects of vortex separation are calculated by the wake-shape iterations performed in the potential flow analysis. The boundary-layer effects are evaluated by using a source transpiration technique via viscous/potential iteration. In discussions of various modeling considerations in simulating the aerodynamic environment around a hub fairing, other essential theoretical background will be provided. Parts of this information are extracted from references 7 to 9.

Simulation with VSAERO from the user's standpoint can generally be divided into two parts: paneling of the body geometry and modeling of the wake. Before beginning the correlation with experimental data, sensitivity studies were conducted to examine the effect of panel density and other parameters. This section first summarizes these configuration related factors which may significantly influence the solutions; then wake models are discussed in details. To illustrate some problems associated with the simulation, H-50, H-160, and a generic hub fairing were used. The midsection profiles of these fairings, along with three other selected for correlation, are displayed in figure 2.

### 2.1 Paneling of Hub Surface

Two options are available in generating the hub fairing surface. One consists of rotating a half section about the hub's centerline to obtain a body of revolution. Figure 3 shows the resulting configuration for a generic hub. This approach is easy to use and it minimizes the error in geometry description. In this case, however, the streamwise direction is radially outward while the spanwise direction is around the azimuth. This definition of direction differs totally from that of the flow, resulting in awkward assembly of the matrix of influence coefficients, which in turn affects the solution significantly. Therefore, this option was not used.

A more appropriate option is to configure the hub fairing in the same fashion as a wing. The fairing was first divided into spanwise stations. Then coordinates at each station were supplied. Because of the high curvature of the hub fairing, this method requires many points to describe the geometry. In the simulations, approximately 2000 points are used for a half configuration, with the exception that only approximately 1200 points are needed for the flat-bottomed hub fairings. The coordinate system and the definition of directions are illustrated in figures 4 and 5. The origin of the reference frame of both geometry description is identical and is located at the center of the hub fairing's lower surface.

During the sensitivity test of panel density, the significant effect of inaccurate geometry description was discovered. In the case of H-50, when the height of one out of the 986 upper-surface coordinates was decreased

by  $0.004 D^1$  (at midchord of the spanwise station at  $0.33 D$  from centerline), the lift and drag coefficients were increased by 0.6% and 1.2%, respectively. The resulting pressure distribution was affected even more, with a maximum difference of 0.03 in  $C_P$  (fig. 6). Note that this decrement in surface coordinates did not cause any real indentation to the fairing surface and could not be detected on a plot of hub-fairing geometry. It can be seen that special caution is required in specifying the coordinates.

Another consideration involved in paneling the hub fairing like a wing is the determination of the number of panels in both streamwise and spanwise direction. For this bluff body, attention must be paid to the panel density around the leading edge to capture the suction and the stagnation zone correctly. In general, each column requires approximately 45 panels on one surface, with panels concentrated around the leading and trailing edge. This density is two to three times higher than that required for a wing-type configuration (refs. 10 and 11).

For this study, a paneling scheme similar to that presented in figures 4 and 5 was employed. Six patches<sup>2</sup> were used to describe a half configuration divided by the plane of aerodynamic symmetry. Between 650 to 900 panels were used for each hub fairing, depending on the hub fairing's curvature and thickness. For the innermost patch on the upper and lower surfaces, each column was further divided into two regions at  $x = 0.3 D$  (after the fairing center). In the region toward the trailing edge, 15 equally spaced panels were used for each column on each surface. This more condensed arrangement allowed better control in adjusting the separation line during the matching process for the jet model. And, this separation pattern description matched the real flow more closely because of the tapering toward the tip instead of an abrupt corner. It also provided sufficient panels near the trailing edge to capture the pressure recovery.

In summary, the panel distribution shown in figure 4 was designed to minimize the number of panels and to make the wake stitching process easier. Meanwhile, the resulting wake characteristics and the overall solutions were also improved.

## 2.2 Determination of Separation Location

The VSAERO solutions depend directly upon where the wake is stitched, which is defined by the flow-separation location. In simulations of hub fairings, this location must be determined not only for the streamwise, but also the spanwise direction. This determination will be discussed next.

**2.2.1 Effective Span-** Unlike a wing-type configuration, the tip vortices from a hub fairing do not shed at the span's end. Instead, the flow curves around the outermost edge (tip) from the bottom surface to the top. This can be observed from the oil-flow-visualization photos presented later. Because of the fairing's circular planform, the vortex separation location cannot be easily determined. Yet, this spanwise location is very important because it governs directly the width of wake sheet. This width in turn fixes the amount of effective lifting area of the body. The term "effective span" will be used in this report to represent the spanwise vortex separation location. The effective span (fig. 7) is the width of the undistorted wake sheet.

The effective span (fig. 8), dictated the calculated magnitude of lift and drag. (Regular wake was used here, but the jet model gave similar results.) As the effective span varied, so did the amount of lifting surface and the resulting lift. The longitudinal sectional profiles of the hub fairing are very similar and are subject to the same angle of attack. Therefore, the lift increment is directly proportional to the effective span at any one  $\alpha$ . For the drag calculation resulting from variation of the effective span, there were no consistent trends.

The effective span used in the simulations was determined both analytically and experimentally. By observing the on-body streamlines from VSAERO output, the spanwise separation locations can be identified. However,

<sup>1</sup> All lengths were nondimensionalized by the hub fairing diameter  $D$ .

<sup>2</sup> A patch is part of a configuration surface consisting of a rectangular array of panels. (See ref. 7 for more definitions.)

this requires an iterative process because the spanwise separation location is directly influenced by the specified width of the wake sheet. From simulation of a generic hub and H-10, this spanwise location is between  $0.35$  and  $0.40 D$  from the centerline. The oil flow visualization performed in the wind tunnel test indicates the spanwise separation location is at  $0.37 D$  for H-50. For a symmetrical fairing similar to H-160, the experimentally determined separation is around  $0.33 D$  from the centerline. Since flow visualization was not obtained for all fairings, an averaged approximation of  $0.36 D$  was used as effective span in all simulations. Note that this representation is acceptable because it is within the uncertainty governed by the finite number of panel columns allowed in simulation.

This effective span ( $0.72 D$ ) may be too large for symmetrical fairings. However, the lift generated by a symmetrical fairing is low for the small range of angles of attack being simulated. Thus its lift should be relatively insensitive to the effective span so that the averaged approximation is justifiable.

**2.2.2 Streamwise Separation Line-** The streamwise separation line is determined by connecting the ends of on-body streamlines calculated by the boundary-layer routines. For the simulations with the regular wake, the streamwise separation line is not needed because the wake is assumed to be shed from the trailing edge. But for the simulations with either the separated wake or the jet model, the separation line is required. Details on streamwise separation location will be presented in section 2.3.3 where the jet model will be discussed more thoroughly.

A problem with early separation on flat-bottomed surfaces was encountered for all three wake models. The boundary-layer calculation indicated that the laminar flow on this surface separated early (close to the leading edge) and was not able to reattach as turbulent flow. A good alternative was to restart the boundary-layer calculation as turbulent flow at a point after the laminar separation location. This program option did not work, however, so the calculation was started again as laminar flow. The VSAERO calculated that the flow on the bottom surfaces stayed laminar until separation. Thus it probably predicted a delayed flow separation and underestimated the skin-friction drag.

In summary, the separation line was restricted to a line for the regular wake and a rectangle for the jet model. Even though a staircase pattern might be closer to real flow separation for the jet model, magnitudes of the resulting solutions were erroneously large. The reason may be due to the great influence of wake panels on each other around the  $90^\circ$  corners formed at the steps.

## 2.3 Wake Modeling

In VSAERO, the flow field is divided into three idealized regions: far field ( $S_\infty$ ), body surface ( $S$ ), and wake ( $W$ ) (fig. 9.) The governing equations are

$$\nabla^2 \Phi = 0 \quad \text{in the flow field} \quad (1)$$

$$\nabla^2 \Phi_i = 0 \quad \text{inside the body} \quad (2)$$

$$\Phi_p = \frac{1}{4\pi} \iint_{S+W+S_\infty} (\Phi - \Phi_i) \mathbf{n} \cdot \nabla \left( \frac{1}{r} \right) dS + \frac{1}{4\pi} \iint_{S+W+S_\infty} \frac{1}{r} \mathbf{n} \cdot (\nabla \Phi - \nabla \Phi_i) dS \quad (3)$$

In simulating hub fairings with VSAERO, the effect of the choice of wake model predominates over other modeling parameters. But since the proper selection was not obvious, three wake models — the regular wake, separated wake, and jet model<sup>3</sup> — were tried. The theoretical formulation of these wake models are outlined below to provide more insight to the problem. Also, problems with application of these wake models are discussed.

<sup>3</sup>Nomenclature is adopted from VSAERO documents (refs. 7 and 8).

The regular wake is based on a thin-wake assumption that its thickness is negligible. The other two wake models include a finite thickness between the wake surfaces. The major differences between the thin and thick wakes are the doublet distribution on the vortex sheet and the method to stitch this vortex sheet (fig. 7). The thin wake consists of a single vortex sheet attached to a separation line (i.e., the trailing edge). The thick wake captures a region of low-energy fluid with its separation line enclosing a group of body panels.

**2.3.1 Regular Wake-** The regular wake is a good model when the actual wake is so thin that the fluid entrainment becomes negligible. In such cases, the wake region collapses into one single-vortex sheet and the jump in the normal velocities across the upper and lower surfaces vanishes. In other words, the source term,  $\mathbf{n} \cdot (\nabla\Phi_U - \nabla\Phi_L)$ , in equation (3) for the wake region disappears. The wake's contribution to the flow equation reduces to

$$\frac{1}{4\pi} \iint_W (\Phi_U - \Phi_L) \mathbf{n} \cdot \nabla\left(\frac{1}{r}\right) dW \quad (4)$$

From the Kutta-Joukowski theorem, the force on an object immersed in a fluid is

$$d\mathbf{F} = \rho \mathbf{V} \times d\Gamma \quad (5)$$

Defining the vorticity vector per unit area to be

$$\boldsymbol{\gamma} \equiv -\mathbf{n} \times \nabla(\Phi_U - \Phi_L) = \frac{d\Gamma}{dW} \quad (6)$$

then

$$d\mathbf{F} = \rho \mathbf{V} \times \boldsymbol{\gamma} dW \quad (7)$$

The force on the wake element  $dW$  becomes zero when  $\mathbf{V} \times \boldsymbol{\gamma} = 0$ . Substituting equation (6) for  $\boldsymbol{\gamma}$  and expanding the resulting triple vector product gives

$$\mathbf{nV} \cdot \nabla(\Phi_U - \Phi_L) - \mathbf{V} \cdot \mathbf{n} \nabla(\Phi_U - \Phi_L) = 0 \quad (8)$$

The load-free condition on the wake is satisfied when both terms in equation (8) become zero. The first term vanishes, (i.e.,  $\mathbf{V} \cdot \nabla(\Phi_U - \Phi_L) = 0$ ), if the gradient of the doublet distribution is zero along the direction of local mean flow. This requires the potential jump to remain constant along the mean streamline in the wake surface; that is,  $\Phi_W = (\Phi_U - \Phi_L) = \text{constant}$ . The second term disappears when the wake panel is aligned with the local velocity so that  $\mathbf{V} \cdot \mathbf{n} = 0$ .

The Kutta condition is implied here when the wake is shed from the trailing edge and  $(\Phi_U - \Phi_L)$  on each wake column is set to be constant to satisfy the load free requirement. Since this constant doublet value is determined by conditions at the point of flow separation, correct location of the separation line is very important. If the regular wake is not stitched to a definitive separation line (or trailing edge), the lift prediction becomes as arbitrary as the user's choice of location (fig. 10). From potential flow theory, moving the separation line toward the lower surface around the "trailing edge" increases the circulation and thus increases the lift. Therefore, this model was used only for hub fairings with sharp edges or symmetrical sectional profiles such that a trailing edge could be assumed without too much ambiguity.

Within the limitation just stated, the regular wake is good for flow without extensive separation. At low to moderate angles of attack when flow separation on the hub fairing is usually small, or sometimes mild, this wake model should be capable of predicting the flow characteristics. Since the regular wake was easy to apply, it was used in simulations of all hub fairings shown in figure 2 (except the generic one).

**2.3.2 Separated Wake-** The separated wake is a thick wake used for extensive flow separation. The vortex sheet of this wake encloses fluid with lower energy level than the rest of the flow field. Instead of one separation line

at the trailing edge, there is one continuous separation line that encloses a section of the upper and lower surfaces at the trailing edge. Although there is a finite thickness between the upper and the lower wake surfaces of the thick wake, the VSAERO formulation is further simplified by assuming no flow entrainment in the wake. This means that the source term,  $\mathbf{n} \cdot (\nabla\Phi_U - \nabla\Phi_L)$ , in equation (3) is again zero as in the regular wake formulation.

Unlike the constant doublet value used in the regular wake, the doublet distribution on the surface of the separated wake is constant spanwise, but varies linearly streamwise. It can be represented by:

$$\Phi_W(s) = \Phi_{sep} + s * \frac{\partial\Phi_O}{\partial s}|_{sep} \quad (9)$$

where  $s$  is measured along each streamline on the wake surface from the separation point. The term  $\frac{\partial\Phi_O}{\partial s}|_{sep}$  is calculated by the program using doublet values of two panels immediately upstream of separation. This means that  $\Phi_{sep}$ ,  $\frac{\partial\Phi_O}{\partial s}$ , and  $\Phi_W$  are calculated for each column, and they are thus functions of spanwise location.

Inside the separated flow region, the pressure distribution on a body is relatively constant. This pressure can be calculated directly as follows:

$$C_{P_{in}} = 1 - \left(\frac{V}{V_\infty}\right)^2 + \frac{\Delta H}{q_\infty} = C_{P_{out}} + \frac{\Delta H}{q_\infty} \quad (10)$$

where  $q_\infty$  is the free-stream dynamic pressure and  $\Delta H$  is the change in total pressure in the separated zone relative to the undisturbed flow;  $\Delta H$  is evaluated as follow:

$$\Delta H = \rho \bar{V} \frac{\partial\Phi_O}{\partial s}|_{sep} \quad (11)$$

with  $\bar{V}$  = average velocity in the shear layer. The separated wake model should best suit the present purpose according to the nature of the fairing's aerodynamic behavior. However, simulations with this model failed when the doublet values diverged during iterations in the matrix solver. Because this model was not recommended by the writer of VSAERO, and because of divergence just noted, investigation of this model was discontinued. Results of the separated wake will not be discussed further in this report.

**2.3.3 Jet Model-** The jet model is also a thick wake. The term "jet" implies that the wake region contains fluid with higher energy; however, the math model turns out to be applicable also to a normal wake, a region with momentum deficit. To simulate the wake behind a hub fairing, the jet model can be thought of as a jet with very small velocity inside the shear layer. Thus instead of high-energy fluid, low-energy fluid is entrained inside the vortex sheet.

Actually, the jet model is a simplified version of the separated wake. Recognizing that  $\frac{\partial\Phi_O}{\partial s}|_{sep}$  in equation (9) is the difference in tangential velocities inside and outside the vortex sheet,  $V_{in}$  and  $V_{out}$ , at the separation line, then

$$\Phi_W(s) = \Phi_{sep} + s * (V_{in} - V_{out})|_{sep} \quad (12)$$

(From this point on, the terms "inner and outer efflux velocity," adopted from the VSAERO output, will be used to refer to the velocity  $V_{in}$  and  $V_{out}$ , respectively). The efflux velocities (fig. 7) are specified on each wake column by the user. This determines the doublet strength on each column according to equation (12).

Recall that the pressure within the wake is:  $C_{P_{in}} = C_{P_{out}} + \Delta H$ . For the jet model, the change in total pressure is calculated by

$$\Delta H = V_{in}^2 - V_{out}^2 \quad (13)$$

The effect of this difference in pressure distribution is included in two places in the program. The first is application of a correction value,  $\Delta H_{ave}$ , to the total pressure in the region of the body inside the wake. Note that  $\Delta H_{ave}$  is

calculated from initially estimated, averaged efflux velocities in the on-body analysis stage. The second correction to the pressure calculation is performed in the wake shape iterations in which  $V_{in}$  and  $V_{out}$  are updated from predicted values of each iteration.

The jet model is closer to the physical flow than the regular wake. But, since the correct magnitudes of the efflux velocities and location of separation are not known at the outset, they are chosen iteratively by matching the estimated to calculated values. The inner loop in figure 11 involves matching efflux velocity pairs while the outer loop matches the separation line. Both processes are discussed in the following subsections.

**Efflux Velocity Matching:** In the simulation,  $V_{out}$  and  $V_{in}$  should be taken from velocities on the body panels immediately before and after the separation line, respectively. To begin the process,  $V_{out}$  was set to some value smaller than the free-stream velocity (say  $0.9 V_{\infty}$ ), while  $V_{in}$  was set to an arbitrary small value ( $0.1 V_{\infty}$  for the present case). After a solution was obtained with these input values, estimated values were matched to calculated values and readjusted if necessary.

Ideally, both  $V_{in}$  and  $V_{out}$  should be adjusted simultaneously. However, the solution was so sensitive to the input efflux velocities that it was impossible to match both at the same time. Therefore,  $V_{in}$  was fixed at  $0.1 V_{\infty}$  in the simulation. To cut down the man-hours required, a computer program was written to automate the matching process.

Even with these simplifications, the process of obtaining a solution was still very long. If the velocity matching did eventually converge ( $V_{out}$  only), it generally required 5 to 15 iterations. Note that the process described above only yielded a solution for a given combination of separation location, angle of attack, number of viscous/potential iteration, etc. Also, the correct separation location was yet to be matched (the outer loop in fig. 11). It could be easily projected that time consumption would accumulate quickly as combinations were varied.

Furthermore, the aerodynamic characteristics predicted with the jet model were very sensitive to the estimated efflux velocities. This sensitivity is demonstrated in figures 12 and 13. Results shown here were for H-50 at an angle of attack of  $0^\circ$  with the location of the separation line chosen according to experimental observation. After the converged solution was obtained, the 14 calculated  $V_{out}$ , corresponding to 14 wake columns, were varied one at a time to generate another solution. Compiling solutions for variations of  $V_{out}$  at different wake columns formed a band of possible error shown in figures 12 and 13. This represented a very serious problem because the lift and drag predictions fluctuated widely for a small change in the magnitude of efflux velocities.

In other words, the intent of figures 12 and 13 is to present the irregular, unpredictable variation of  $C_L$  and  $C_D$  due to a slight difference in one of the 14 estimated  $V_{out}$ . For example, although a greater change in  $V_{out}$  usually resulted in a larger deviation, the trend was not consistent. A 2% decrease in one  $V_{out}$  may have a stronger influence on the solution than a 10% decrease in another one. And in terms of selecting an estimated  $V_{out}$ , no one wake column could be identified as most influential to the solution.

Note that the predicted  $C_L$  of 0.1022 and  $C_D$  of 0.0171 from the converged solution (at 0% in figs. 12 and 13) were too low when compared with experimental values of 0.2529 and 0.0287, respectively. Additionally, the large deviation, (-14 to 43% for  $C_D$  and -39 to 7% for  $C_L$ ), was due to a change within a range  $\pm 10\%$  of final calculated  $V_{out}$ , which was only 5 to 9% of magnitude of  $V_{\infty}$ . Then since the convergence criterion in matching was within  $\pm 10\%$  of  $V_{\infty}$ , it could be seen that the converged solution was not necessarily accurate. Because the above observation was for varying only one  $V_{out}$ , it might be projected that the uncertainty would be greatly compounded when all efflux velocities pairs were considered.

One possible explanation for such sensitivity to efflux velocities was the steep spanwise pressure gradient expected for such a low-aspect-ratio configuration with a high surface curvature. This could be observed from figure 6 (spanwise pressure distribution at hub center) and figure 14 (pressure distribution immediately before separation). As a result, any change in efflux velocities not only affected the body and wake columns to which they are assigned, but also the whole flow field around the hub fairing.

In the process of iterating for a converged solution, results from run to run were very likely to fluctuate in a similar manner to that demonstrated in figures 12 and 13.

Although it probably would take only 10 to 20 trials to obtain a converged solution, instead of as drastic as 140 shown in the figure, this figure still reflected the large time requirement of using the jet model.

**Separation Line Matching:** The separation line for a jet model was not assumed to be at the trailing edge. Since it was not known initially, the estimated separation line also had to be matched to that predicted by VSAERO. This process was not as time-consuming as that for the efflux velocities. Also, there were two criteria to guide this process.

First, the value of the shape factor  $H$  from the boundary-layer calculation was checked. To refresh the reader,

$$H = \frac{\delta^*}{\theta} \quad (14)$$

where  $\delta^*$  is the boundary-layer displacement thickness and  $\theta$  is the momentum thickness. The shape factor can be interpreted as a measure of the adverse pressure gradient. In turbulent flow, separation occurs approximately at  $H = 2.4$  (ref. 12). For the simulations, flow is considered separated if the shape factor is between 2.0 and 2.5.

Another check for separation line location when using the jet model is the transition of chordwise pressure distribution before and after the separation line. The variable  $C_p$  should increase at the separation point and remain relatively constant thereafter. However, an overshoot in calculated pressure just ahead of separation is likely to result when the efflux velocities do not match well. In such cases, the boundary-layer calculation always predicts an earlier separation than the original estimate. This will either make the matching process endless or yield erroneous solutions.

In summary, the computation time for a regular wake run was between 250 and 500 sec on a Cray X-MP computer, depending on the number of body and wake panels and the number of wake shape iterations. The computation time for each jet model run was below 300 sec because only one wake-shape iteration was used. But, because of the two additional iterative loops required by the jet model (fig. 11), using this option was actually much more costly. A jet model solution would take up to 20 trials to match both efflux velocities and separation locations; beyond this the matching would not be pursued. Thus, an average of over 40,000 Cray sec was required in using the jet-model option to simulate one hub fairing for seven different angles of attack.

Although the jet model was not very efficient and accurate, it was still used in the correlation study because preliminary investigation indicated that some results using the regular wake were even less accurate.

**2.3.4 Other Wake Modeling Parameters-** In addition to wake model choice, several wake-related parameters have direct influence on the VSAERO solutions. One of them is the length of the wake sheet. As a general rule, this length should be five times an appropriate reference length. For the hub fairing simulations, five diameters was used.

Another important wake parameter is the location of wake grid planes which determines the wake panel distribution in the streamwise direction. This distribution may significantly affect the solution, especially when the wake is stitched ahead of some body panels (i.e., not at the trailing edge). To alleviate this problem, the wake grid planes should be matched to the control points of body panels. In other words, the length of body panels and wake panels in the vicinity of the separation line should be approximately equal so that the influence of the wake and the body can be evaluated properly. This selection is also partly based on the fact that velocities on wake panels are calculated at wake grid planes instead of their control points. However, the implementation of this guideline in the present simulation was not straight-forward because the control points for panels in the same "row" vary greatly at the trailing edge (because of the circular planform). In the simulation, wake grid planes were distributed according to the locations of each column's last control point. (Orientation of row and column is illustrated in fig. 4.)

Inspection of figure 15 reveals that the regular wake solution was not as sensitive to wake panel density as the jet model. This might be because the regular wake was stitched at the trailing edge and the doublet strength on each wake panel was constant. On the other hand, the jet model solution was more sensitive because of the overlapping wake and body panels and the streamwise linear variation of doublet strength. The left-most data points in figure 15 with wake panel length of  $0.02 D$  corresponded to the wake panel density used in the simulations.

The number of wake-shape iterations is also very important. During each iteration, VSAERO relaxes the wake sheet and aligns the wake panels with the local velocities. Note that the requested number of wake shape calculations is performed only in the first viscous/potential iteration. In each subsequent iteration, the wake is relaxed once. The number of iterations required strongly depends on the number of panels. For the regular wake, most solutions would converge within three iterations. For the jet model, however, the doublet solution diverged if the wake was relaxed more than once. The number of wake shape iterations was consequently limited to one for the jet model. The number of viscous/potential iterations was limited to one in all simulation because otherwise the solution would fluctuate.

### 3 CORRELATION OF VSAERO RESULTS WITH TEST DATA

Five small-scale hub fairings that were tested recently in the 7- by 10-Foot Wind Tunnel at NASA Ames Research Center were selected for correlation (ref. 6; Graham, D. R.; Sung, D. Y.; and Young, L. A.: A Small-Scale Investigation of Helicopter Hub and Pylon Fairing Drag Characteristics. To be published as NASA TM-101052). The sectional profile of these fairings, designated H-10, H-50, H-130, H-150, and H-160, are shown in figure 2. All hub fairings were chosen to have sharp edge and/or symmetrical sectional profile to expedite the investigation of the aforementioned wake models.

The sharp-edged fairings were chosen instead of the blunt- (round-) edged fairings to provide a well-defined location for stitching the regular wake. This well-defined trailing edge ensured that the Kutta condition would be applied correctly. When the jet model was used, the estimated separation line had to be matched to that predicted by the program on both the upper and lower hub surfaces. The difficulties involved dictated that only fairings with symmetrical profiles be simulated.

Aerodynamic load data for these hub fairings were correlated with VSAERO predictions for angle of attacks from  $-4$  to  $2^\circ$ . Additionally, flow visualization data were compared qualitatively with VSAERO solutions for H-50 and H-160. Lift and drag data are presented in the form of respective dimensionless coefficients; the reference area is hub-fairing planform area. All lengths and velocities were nondimensionalized by fairing diameter and free-stream velocity, respectively.

#### 3.1 Quantitative Correlation

The experimental data consisted of measured lift and drag force on the isolated nonrotating hub fairings. After the tare force on the sting support was subtracted, these data were nondimensionalized by the planform area of the fairing. The tests were conducted at a dynamic pressure of  $40 \text{ lb}/\text{ft}^2$ . This condition corresponded to a free-stream Mach number of 0.16 and a Reynolds number based on fairing diameter of  $1.07 \times 10^6$ . More details about the test can be found in Graham's NASA TM to be published.

The range of angles of attack being tested was from  $-3^\circ$  to  $0^\circ$ . Consequently, the VSAERO simulation was limited to a range of  $-4^\circ$  to  $2^\circ$ . This slightly larger range was used to observe the trends of the VSAERO predictions.

Though the primary interest of this validation is drag prediction, lift correlations are still used as the first step in evaluating the applicabilities of VSAERO for hub fairings. Lift is emphasized because its calculation should be more accurate than that of drag for a potential flow code. Also, drag predictions are deemphasized because the integral boundary-layer method used by VSAERO cannot fully account for the viscous effect and cannot predict the interference drag arising from the aerodynamic interaction of the fairing and the sting. (As mentioned before, the sting was not simulated).

**3.1.1 Lift Correlation-** The lift data of five hub fairings are correlated in figures 16 – 20. Four types of results were obtained for the current study: potential and viscous solutions for both the regular wake and the jet model. The solutions are compared to illustrate various characteristics resulting from different VSAERO simulation options. Since not all types of solutions were of interest, for clarity, not all solutions are shown. Also, note that scales used for  $C_L$ ,  $C_D$ , and  $\alpha$  are identical in all plots. Correlation is discussed on a configuration basis.

**H-10** — For this configuration, the viscous solution using a regular wake and the potential solution using a jet model are plotted with the experimental data in figure 16. Since the viscous lift solution is always smaller than that of potential solution for the regular wake, it is conservative to conclude that the potential jet model correlates better than both the potential or the viscous regular wake. This conclusion supports the idea that separation on the hub fairing is not negligibly small even for such a streamlined configuration as H-10.

**H-50** — This configuration has a flat bottom surface which caused the laminar separation problem described earlier. Both experimental data (flow visualization) and VSAERO results (with restart option for boundary-layer calculation as laminar flows) indicated that separation on the bottom surface occurred very close to the trailing edge. When stitching the wake using the jet model, the lower separation point was taken at the sharp edge while the separation line on the upper surface was adjusted according to the VSAERO prediction. This approach failed because the predicted upper separation line always stayed ahead of the prescribed one. Consequently, the jet model was not used in this correlation.

For H-50 using the regular wake, it seemed like the potential calculation correlated better than that with viscous effect. It should be pointed out that including the viscous effect in the regular wake always reduces the magnitude of the predicted lift, as can be seen in figure 17. This may be due to boundary layer growth which in effect reduces the curvature, and thus camber, of the fairing, especially toward the trailing edge.

Significant discrepancy between the lift curve slopes is exhibited in figure 17. As noted from figure 8, the lift curve slope remained constant even as the effective span was varied. Since there were no other known causes, the difference was believed to come from the inaccurate calculation of the three-dimensional effects on this “low-aspect-ratio” lifting body. For example, the calculated induced velocities might be incorrect such that the effective angle of attack was reduced, which in turn lowered the lift. This problem probably is associated with the poor geometric modeling of the hub fairing with this panel code.

**H-130** — This configuration also has a flat-bottomed surface and similar behavior to that of H-50 was displayed here. This configuration confirmed the previous conclusion that the potential calculation generally predicted better than viscous calculation in lift. And the magnitude of lift is lowered by boundary-layer effects (fig. 18).

The VSAERO lift curve with viscous effect showed slightly irregular behavior which suggested that there existed uncertainty in calculating the viscous effects. Lastly, possibly for the same reasons suggested for H-50, the slopes of both curves differed from experimental value significantly.

**H-150** — This symmetrical fairing resembles a slab of a circular cylinder and has a more pronounced three-dimensional effect. Four curves are presented in figure 19 for this configuration: potential and viscous solution of the regular wake, potential solution of the jet model, and experimental data.

Though the symmetry line on the blunt edge allows the regular wake to be stitched with minimized arbitrariness, it does not represent a true trailing edge. The flow is likely to separate before turning from the nearly

flat surface onto the blunt edge. Moreover, as the angle of attack was varied, the circulation around the fairing also changed, and thus the separation line assumed for the regular wake *should* also be adjusted. But, since the amount of movement could not be determined by the program, the location of this separation line was fixed at the symmetry line.

Both regular wake solutions revealed that neither the correct magnitude nor slope was predicted. (Note the irregular behavior of the regular wake viscous solution, especially at  $\alpha = -3^\circ$  and  $-4^\circ$ .) Inspection of the drag correlation also suggests that the separation at the blunt edge is too large for the thin-wake assumption made in the regular-wake formulation.

Resulting from more extensive separation than the other fairings, the jet model predicted better than the regular wake for H-150. Note that the jet model lift prediction reflected about  $\alpha = 0$  with a change in sign. Recall that this should be true because of the fairing's symmetry. On the other hand, the experimental lift was not zero at  $\alpha = 0^\circ$ . This suggested that there might be errors in the data acquisition or the experimental setup.

**H-160** — This is a hub fairing with a symmetrical sectional profile and a definitive edge. All wake options were investigated for this configuration. Presented in figure 20 are the viscous solution of the regular wake, potential and viscous solution of the jet model, and experimental data. Unlike the regular wake, the lift prediction by the jet model is higher if viscosity is included. This erroneous trend may be interpreted as showing the importance of selecting a correct separation line when the jet model is used. (Recall that the regular wake just assumes separation at the trailing edge.)

Similar to H-150, the experimental zero lift is not at  $\alpha = 0$  for this configuration. This made determining the accuracy of different methods difficult. The viscous solution using both the regular wake and the jet model were relatively close if the data point of the jet model at  $\alpha = -2$  was neglected. In this case, the regular wake model would be superior because it was simpler to apply and it eliminated the uncertainties in efflux velocity matching.

**3.1.2 Drag Correlation-** Since the drag values from the potential solution only represents the induced drag (drag caused by lift), simulations with such option are not included in this correlation study. Viscous solutions for both the regular wake and the jet model are compared in figures 21–23 with experimental data and are discussed below. The presented drag calculation includes induced drag, skin-friction drag, and pressure drag. Experimental drag data for H-10 and H-130 are not available; hence no correlation is presented.

**H-50** — The jet model solution could not be obtained for this configuration due to the reasons discussed in section 3.1.1. For the regular wake, the drag correlation was quite good (closer than its lift correlation). As discussed in section 2.2.2, the drag may be underestimated because the flow on the bottom surface is calculated as laminar until separation, instead of transiting to turbulent as it should be.

Nevertheless, this seemed to suggest that overall aerodynamic prediction using the regular wake with viscous effects might be acceptable for a hub fairing with a sharp trailing edge.

**H-150** — Both the regular-wake and the jet-model solutions are presented here. With all conditions unchanged (except the angle of attack), the boundary-layer calculation broke down at  $\alpha = -3^\circ$  and  $-4^\circ$ . As a result, the predicted drag values were high at these angles of attack (fig. 22). This once again confirmed that the thin-wake assumption for this bluff configuration was not valid. On the other hand, the jet-model drag prediction was also unacceptable because its magnitude was 100% higher than the experimental value.

**H-160** — Among all selected hub fairing configurations, H-160 represented the most ideal model for simulation. However, its drag correlation showed that VSAERO did not predict drag accurately and consistently. Opposite to the observation made for H-50, the drag value predicted by the regular wake was too high (off by almost 0.05 in  $C_D$ ). For the jet model, the drag prediction was much closer to the test data.

As can be seen from drag correlations for the three configurations, there are no consistent methods to predict hub-fairing drag.

## 3.2 Qualitative Correlation

Two flow visualization techniques, laser sheet and oil flow, were used to investigate the flow pattern on the hub fairing and in the wake region. Details about the experimental setup can be found in Graham's NASA TM to be published.

**3.2.1 Oil Flow Visualization-** This technique was used to observe the flow separation pattern on the hub fairing by detecting the reflection of ultraviolet light off the oil accumulated in the vicinity of the separation line. Presented in figure 24 is a photograph of H-160 at an angle of attack of  $0^\circ$ . The separation pattern predicted by VSAERO (using a regular wake) is presented in figure 25 for comparison. This pattern was formed by joining the ends of the on-body streamlines (dashed lines shown in figure). From the top view, the experimental and calculated separation lines correlated remarkably well. The flow observed from both figures seemed to remain attached to the surface almost to the trailing edge. But, when the curvature at the hub fairing edge was taken into consideration the wake was actually quite thick (fig. 26). From the photographs and observations made during the test, the spanwise separation location was approximately at  $0.4 D$ .

**3.2.2 Laser Sheet Flow Visualization-** This technique was used to investigate the vortex sheet roll up in the wake region. The vortices were visualized with a scan plane formed by a sheet of laser light. These planes were nearly perpendicular to the flow direction. The vortices roll up was also simulated by VSAERO, using a regular wake (fig. 27). The plane of dots shown in this figure was a scan plane corresponding to one of the laser sheet locations. Note that experimental flow visualization runs were only performed for hub fairings in the presence of a shaft fairing and a fuselage. Although the aerodynamic interference from the shaft fairing and fuselage would affect the strength and the location of the vortices, the scan planes were selected sufficiently far away downstream to minimize this effect.

The H-50 was selected for correlation. The VSAERO and experimental results can be compared in figures 28-30. The scan planes were chosen at distances of  $1.02$  and  $1.55 D$  behind hub center. Note that the scan planes for the laser flow visualization were slightly slanted. The first and second station planes were  $13.3^\circ$  and  $-1.2^\circ$  off, respectively. (The positive angle was measured clockwise between the perpendicular to the flow direction and the scan plane). As a result, the pair of vortices shown in the photograph differs slightly in size.

Inspection of figures 28-30 showed that the experimental and analytical vortex core locations agreed quite well. In addition, the vortex diffusion in the flow direction can be observed from these figures.

## 4 CONCLUSION

In simulating helicopter hub fairings with VSAERO, special consideration must be given to the paneling density and method to model the hub geometry, effective span, streamwise separation location, and wake-panel density. These factors have a significant effect on lift and drag prediction. But even if all these concerns are addressed within the capabilities of the code, the flow cannot be modeled satisfactorily.

The jet model was a more appropriate model overall than the regular wake, especially for fairings with a blunt edge. However, a problem was associated with the jet model: the unsuccessful matching of the estimated and the calculated efflux velocities. The required, long, iterative process did not guarantee a converged solution. Hence, the regular wake was preferable if the hub fairing had a definite, sharp edge for wake stitching. In any case, neither the jet model nor the regular wake yielded satisfactory results. Additionally, the sensitivity in matching of efflux velocities made a definite, reliable solution virtually impossible.

Since the overall correlation was inconsistent and poor (especially the drag coefficient) and the computational time and man-hours required were great, the author recommends that VSAERO not be used for designing

low-drag helicopter hub fairings. Other analytical tools should be investigated for this objective. One such potential tool may be CFD codes that solve the Navier-Stokes equations and have the capability to predict aerodynamic characteristics accurately at low Mach numbers.

## REFERENCES

1. Stroub, R. H.; and Rabbott Jr., J. P.: Wasted Fuel - Another Reason for Drag Reduction. Special Report 31st AHS National Forum. Washington, D.C., May 1975.
2. Keys, C. N.; and Rosentein, H. J.: Summary of Rotor Hub Drag Data. NASA CR-152080, 1978.
3. Sheehy, T. T.: A Method for Predicting Helicopter Hub Drag. USAAMRDL-TR-75-48, 1975.
4. Felker, F. F.: An Experimental Investigation of the Hub Drag on the XH-59A. AAIA Paper 85-4065-CP, October 1985.
5. Young, L. A.; and Graham, D. R.: Experimental Investigation of Rotorcraft Hub and Shaft Fairing Drag. AAIA Paper 86-1783-CP, June 1986.
6. Young, L. A.; Graham, D. R.; Stroub R. H.; and Louie, A. W.: Reduction of Hub and Pylon Fairing Drag. Presented at the 43rd AHS Annual Forum, St. Louis, Mo, May 1987.
7. Maskew, B.: Program VSAERO – A Computer Program for Calculating the Non-Linear Aerodynamic Characteristics of Arbitrary Configurations (User's Manual). NASA CR-166476, 1982.
8. Maskew, B.: Program VSAERO – A Computer Program for Calculating the Non-Linear Aerodynamic Characteristics of Arbitrary Configurations (Theory Document). Analytical Methods, Inc., Redmond, Washington, December 1984.
9. Maskew, B.; Rao, B. M.; and Dvorak, F. A.: Prediction of Aerodynamic Characteristics for Wings with Extensive Separations. Paper No. 31 in Computation of Viscous-Inviscid Interactions, AGARD CP-291, February 1981.
10. van Dam, C. P.: Swept Wing-Tip Shapes for Low-Speed Airplanes. SAE Paper 851770, October 1985.
11. Martin, D. M.; and Stroub, R. H.: VSAERO Analysis of Structurally Decoupled Tip Planforms for a Semispan Wing. AIAA Paper 87-2416-CP, August 1987.
12. White F. M.: Viscous Fluid Flow. McGraw-Hill Book Company, 1974.

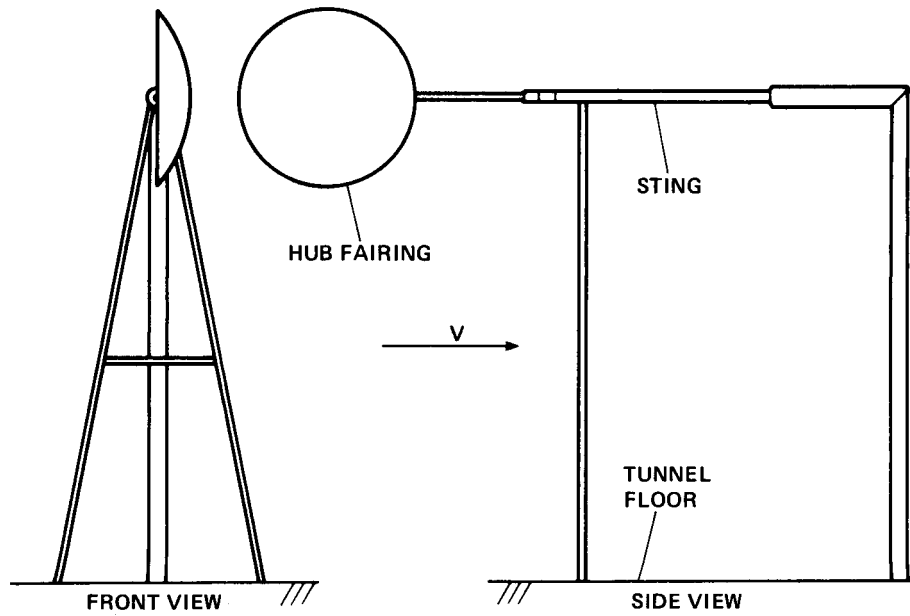


Figure 1.- Sting support used in the wind tunnel tests of isolated helicopter hub fairings.

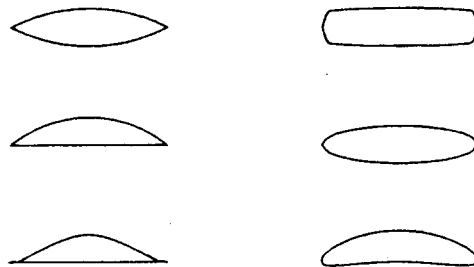


Figure 2.- Sectional profiles of hub fairings selected for correlation.

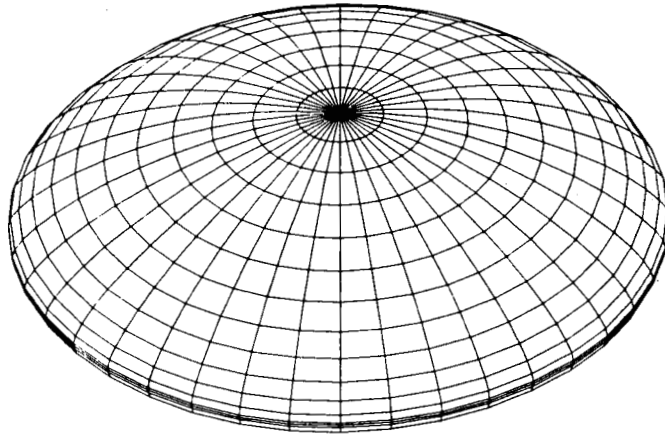
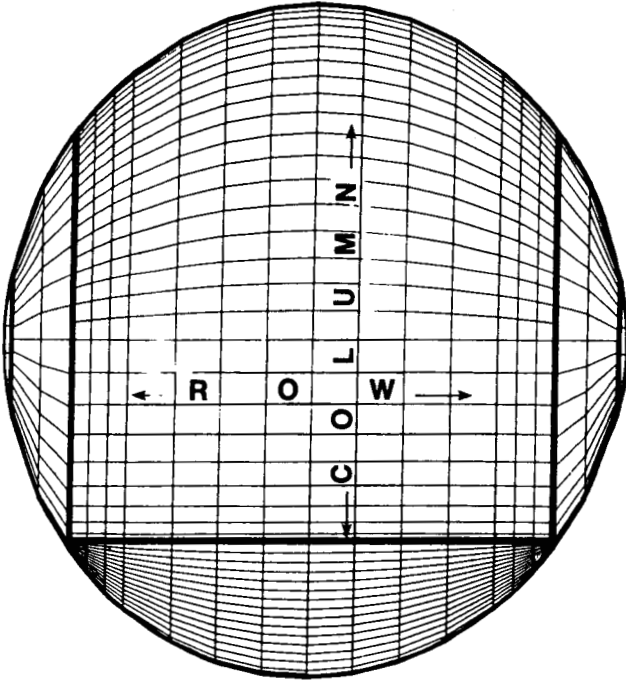


Figure 3.- Hub configuration generated by the body-of-revolution method (generic hub).



PATCH OUTLINE

Figure 4.- Final configuration for H-50 (planform view).

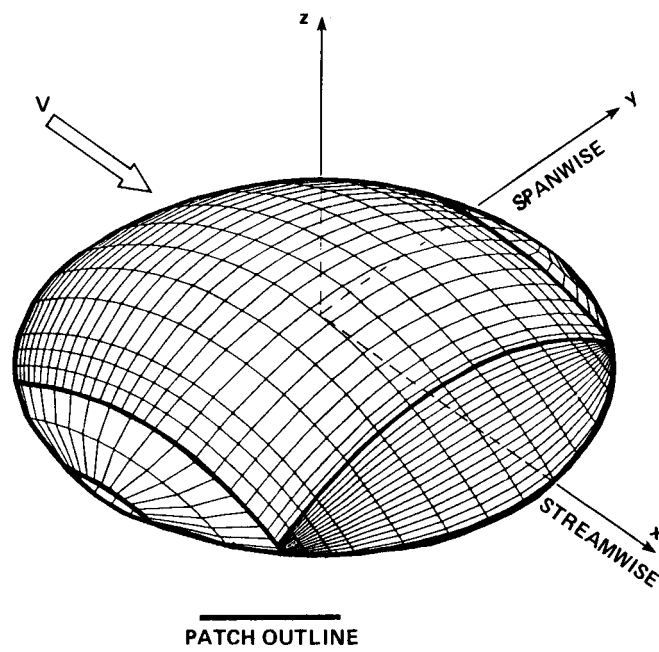


Figure 5.- Final configuration for H-50 (oblique view).

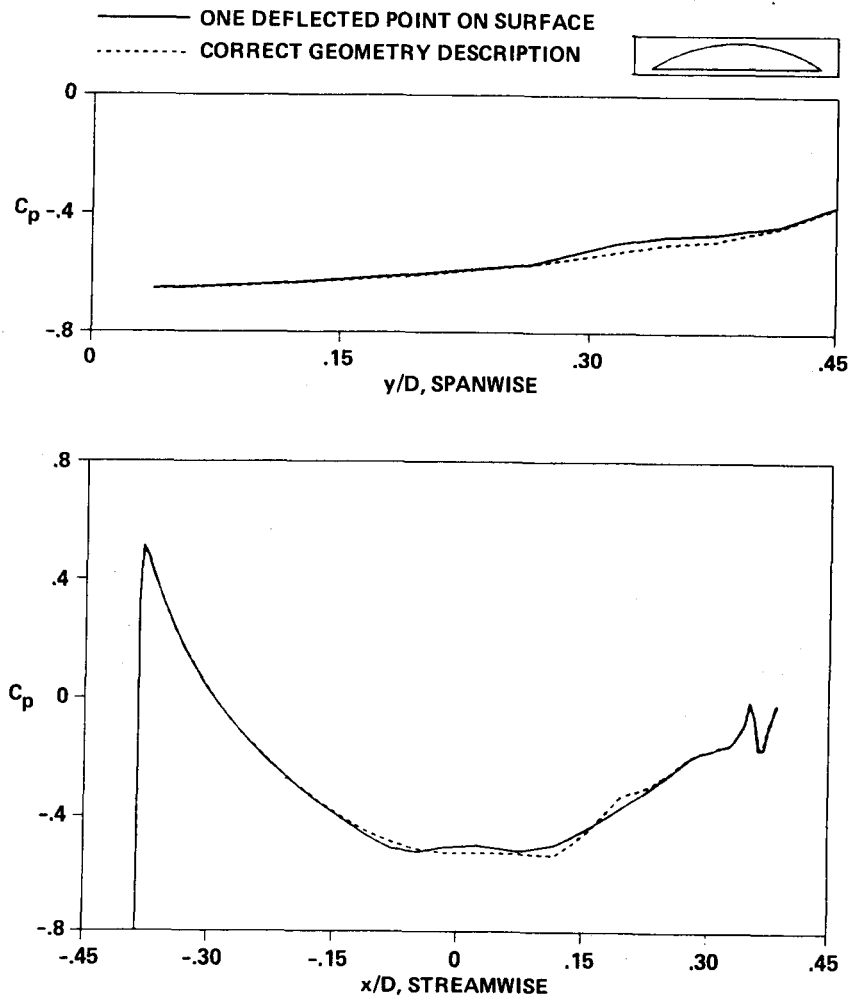


Figure 6.- Sensitivity of pressure distribution to slight geometry change (H-50).

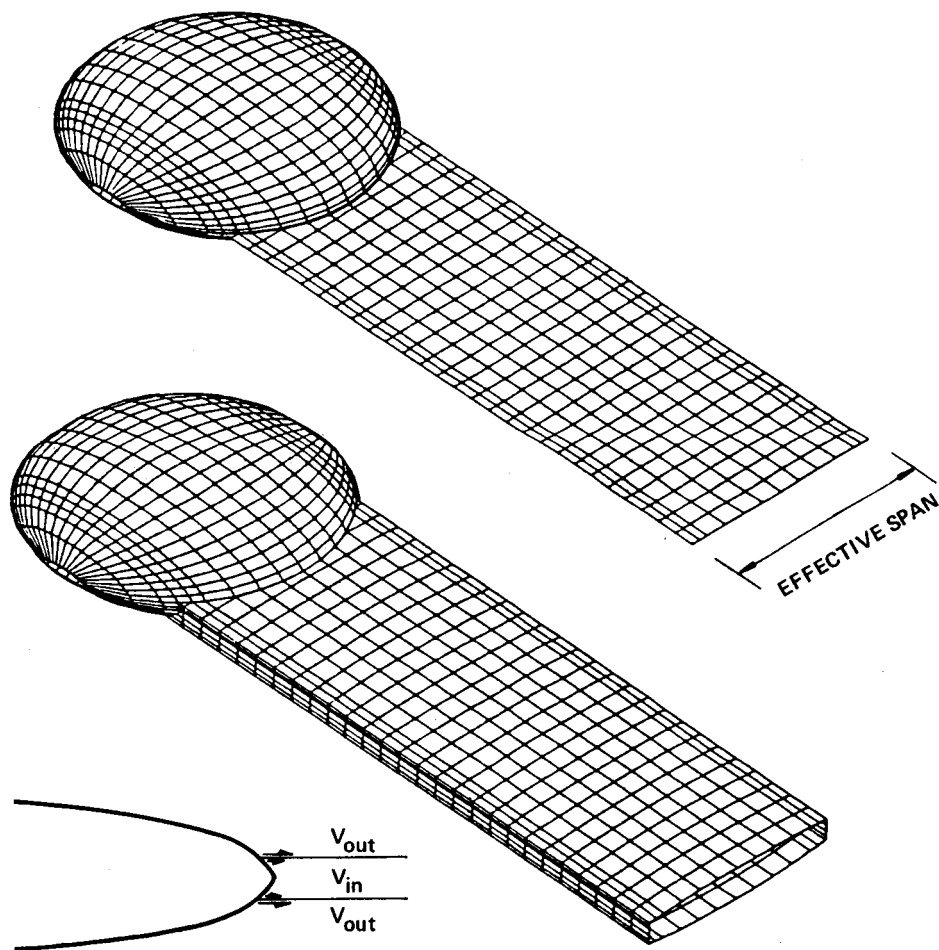


Figure 7.- The thin wake (top) and thick wake with efflux velocity pairs illustrated (bottom).

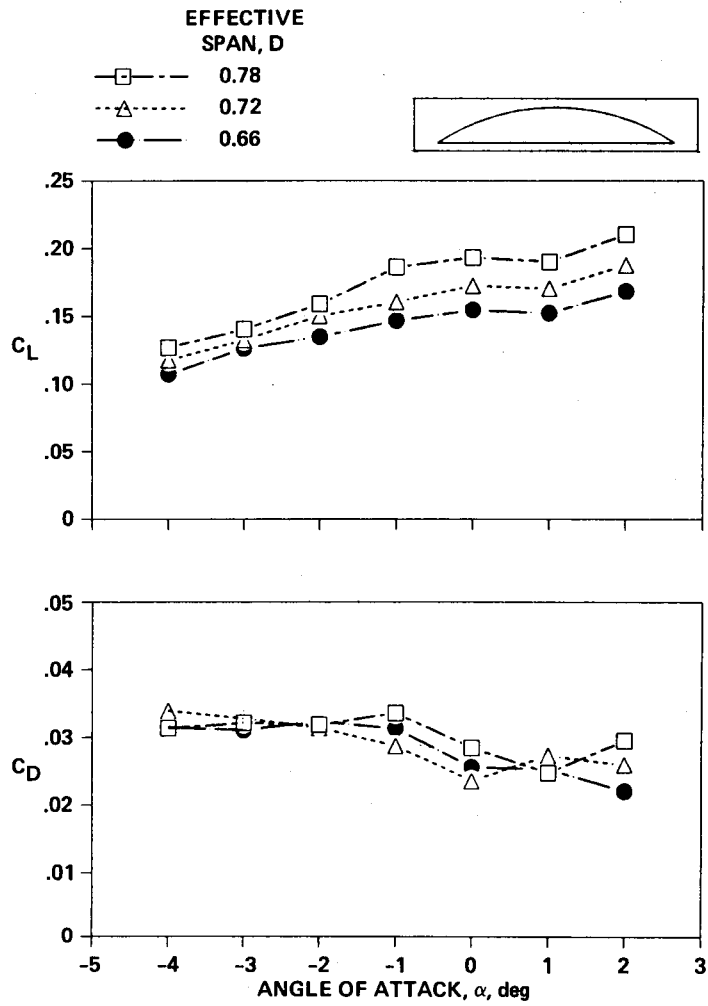


Figure 8.- Lift and drag variation due to effective span (H-50).

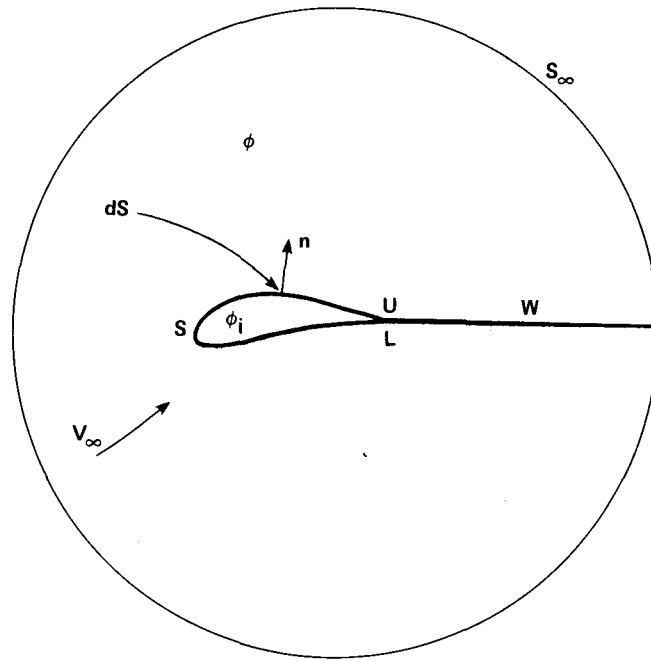
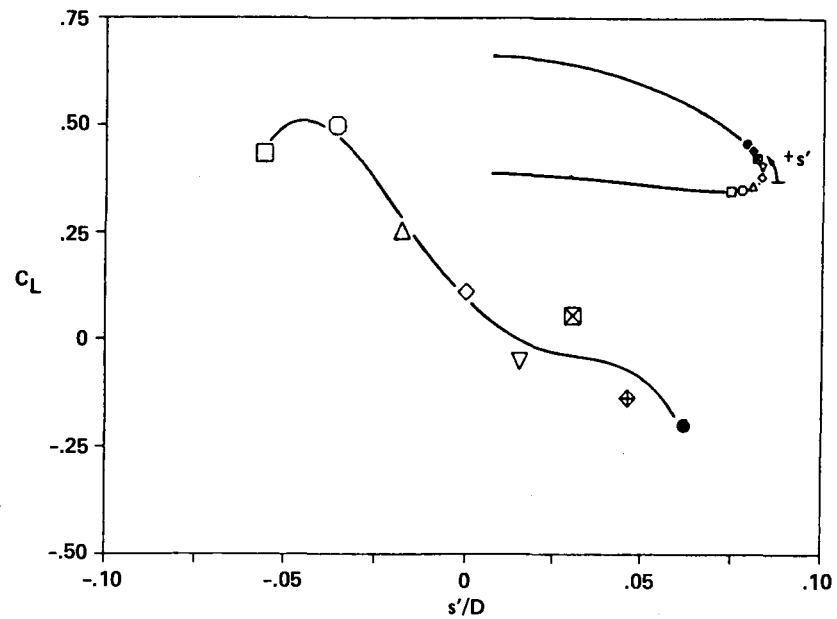


Figure 9.- Idealized flow model used in VSAERO <sup>5</sup>.



Note:  $\frac{s'}{D}$  corresponds to the non-dimensionalized distance on the hub surface with reference to zero value shown in the contour plot. Different data symbols on the lift curve correspond to the positions indicated on the contour plot with the same data representation.

Figure 10.- Variation of lift due to regular wake stitched at different locations on round edge (generic hub at  $\alpha = 0^\circ$ ).

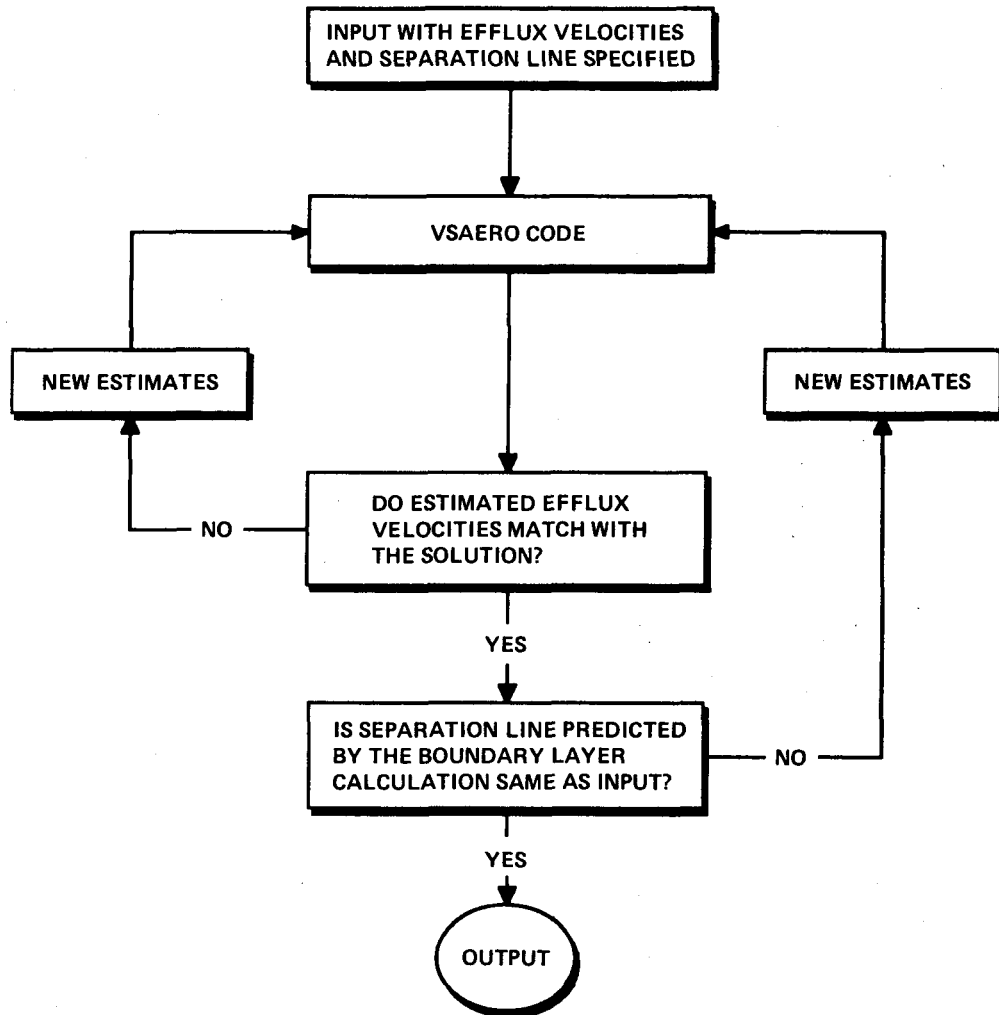
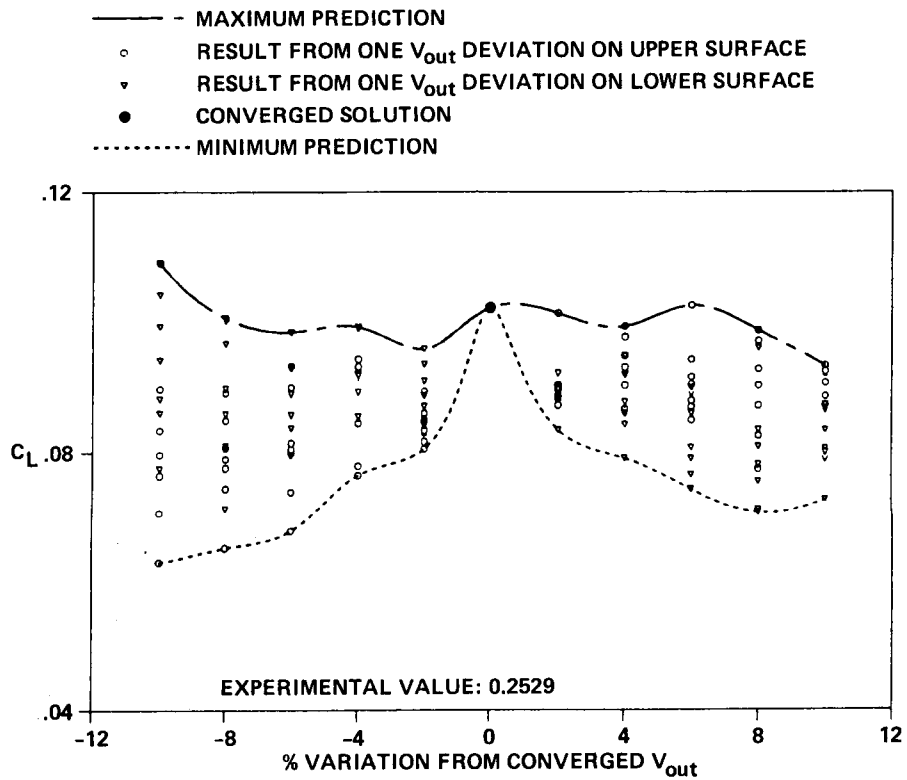


Figure 11.- Iteration loop for analysis with the jet model.



Note: there are 10 variations in magnitude for each one of the 14  $V_{out}$  (corresponds to 14 wake columns), making the total number of runs 140. (Same is true for plot presented on next page.)

Figure 12.- Sensitivity of lift prediction to changes in efflux velocities (H-50).

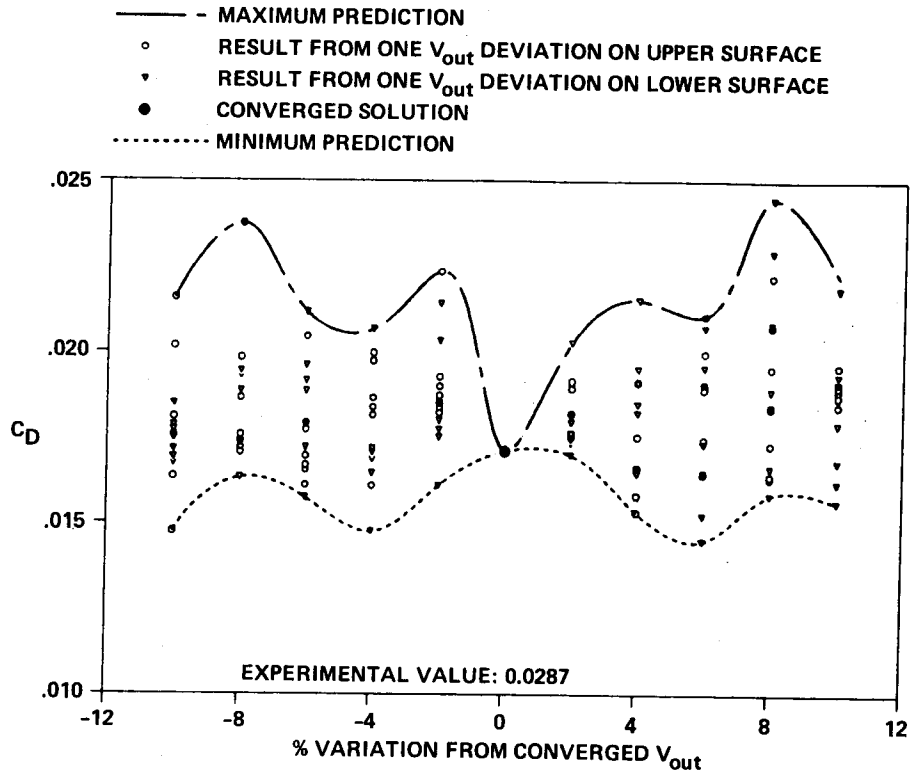


Figure 13.- Sensitivity of drag prediction to changes in efflux velocities (H-50).

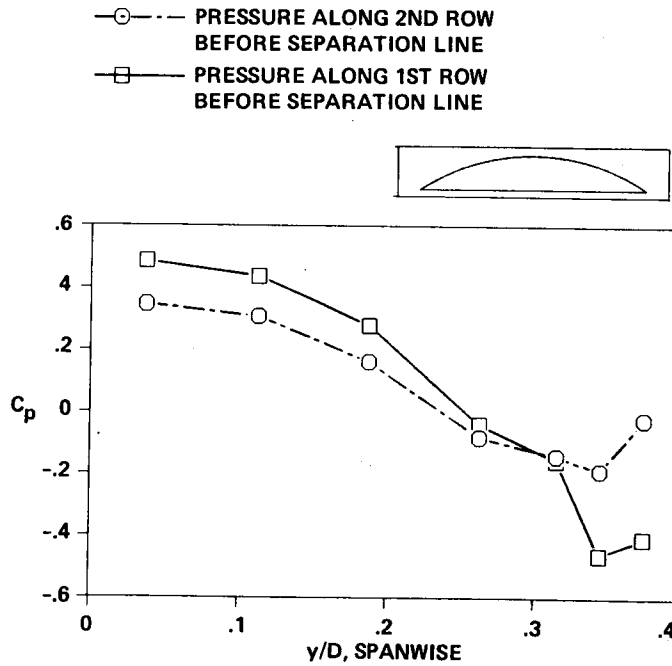


Figure 14.- Pressure distribution before separation (H-50).

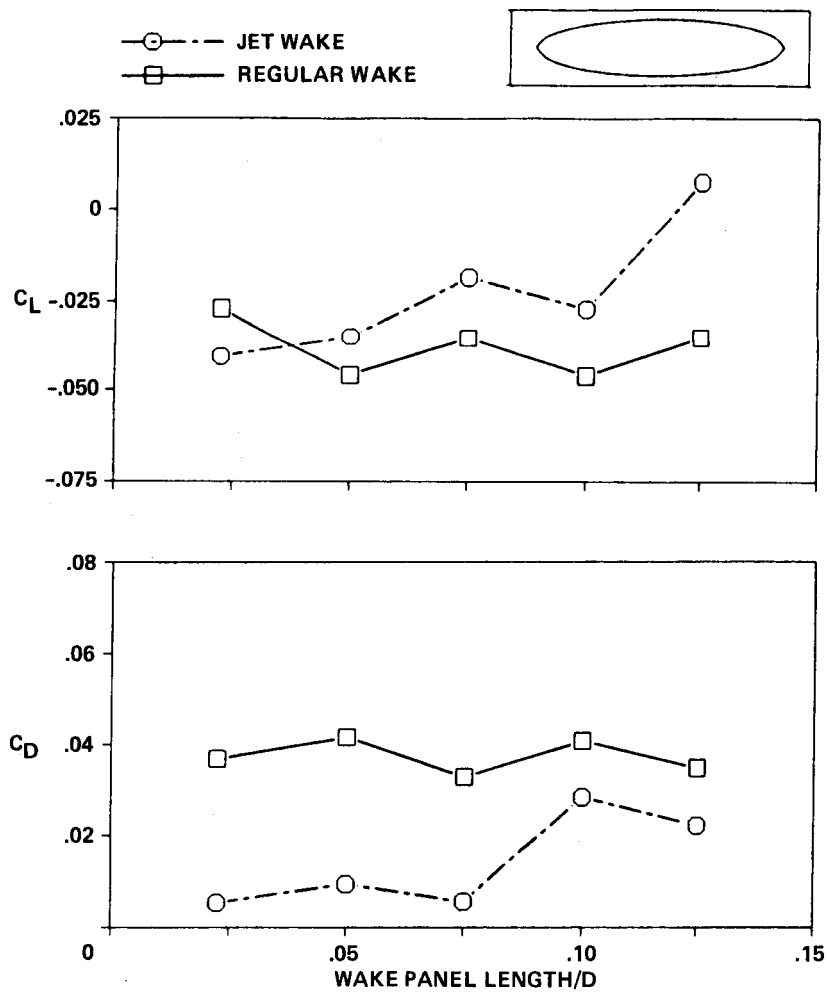


Figure 15.- Lift and drag variation due to wake panel density (H-160 at  $\alpha = -4.^\circ$ ).

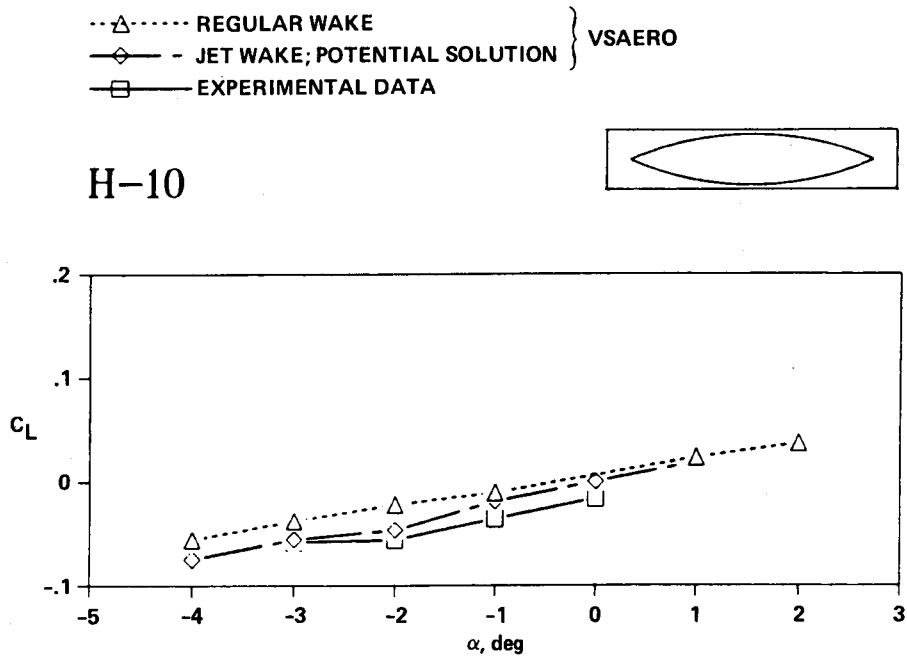


Figure 16.- Lift correlation of H-10.

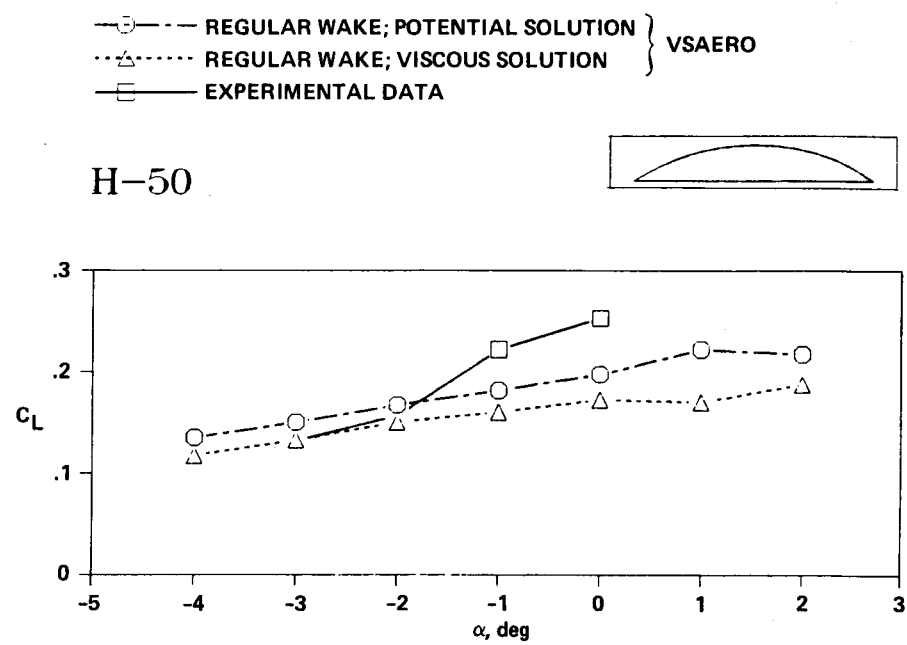


Figure 17.- Lift correlation of H-50.

- REGULAR WAKE; POTENTIAL SOLUTION
  - △--- REGULAR WAKE; VISCOUS SOLUTION
  - EXPERIMENTAL DATA
- } VSAERO

H-130

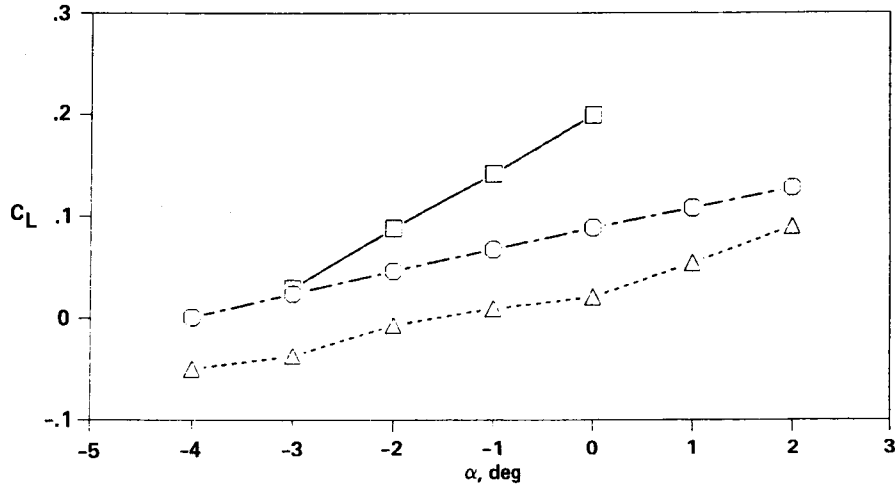
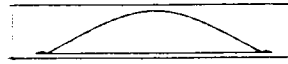


Figure 18.- Lift correlation of H-130.

- REGULAR WAKE; POTENTIAL SOLUTION
  - △--- REGULAR WAKE; VISCOUS SOLUTION
  - JET WAKE; POTENTIAL SOLUTION
  - EXPERIMENTAL DATA
- } VSAERO

H-150

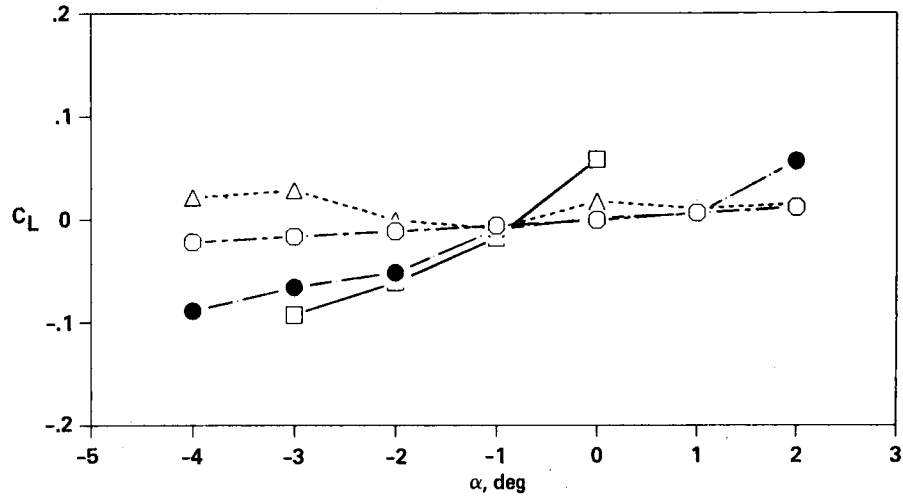


Figure 19.- Lift correlation of H-150.

- △--- REGULAR WAKE; VISCOUS SOLUTION
  - ◇--- JET WAKE; POTENTIAL SOLUTION
  - JET WAKE; VISCOUS SOLUTION
  - EXPERIMENTAL DATA
- } VSAERO

H-160

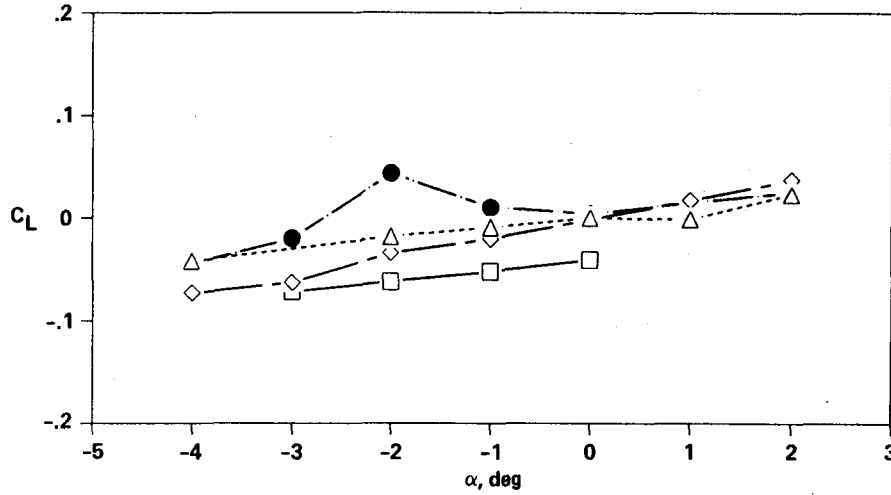
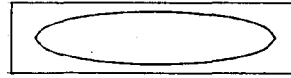


Figure 20.- Lift correlation of H-160.

- △--- VSAERO, REGULAR WAKE
- EXPERIMENTAL DATA

H-50

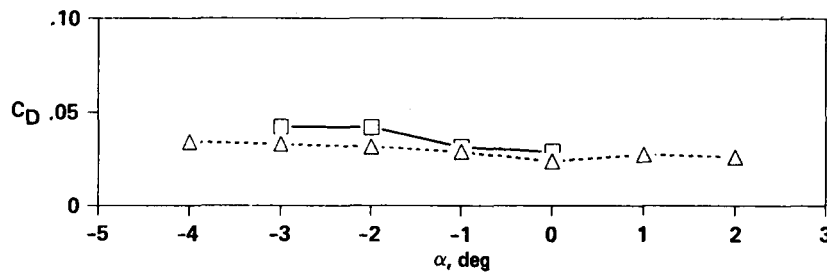
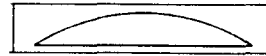


Figure 21.- Drag correlation of H-50.

---△--- REGULAR WAKE } VSAERO  
 ●--- JET WAKE }  
 □--- EXPERIMENTAL DATA



H-150

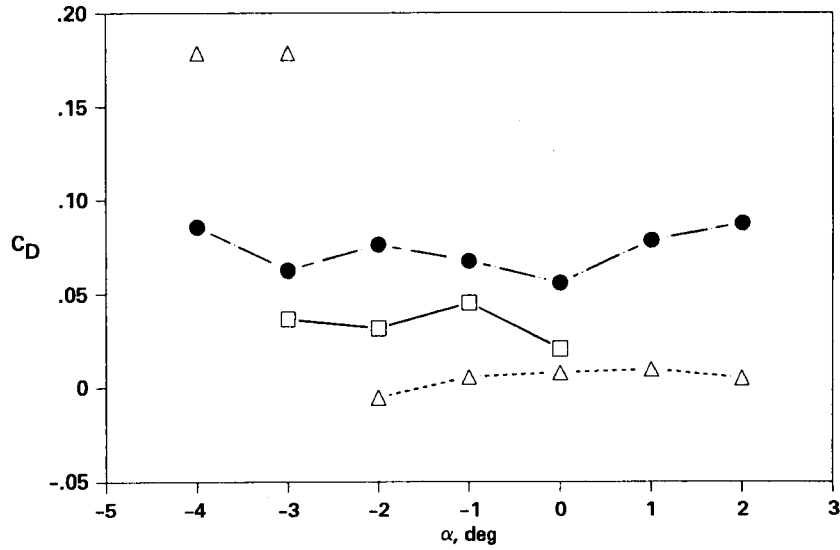
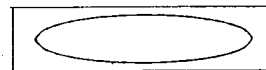


Figure 22.- Drag correlation of H-150.

---△--- REGULAR WAKE } VSAERO  
 ●--- JET WAKE }  
 □--- EXPERIMENTAL DATA



H-160

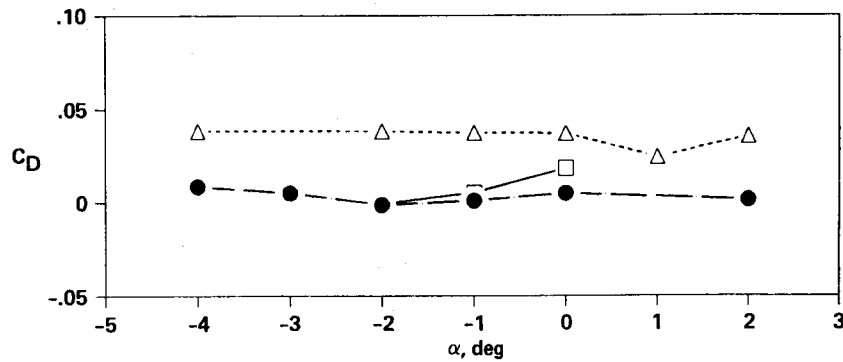


Figure 23.- Drag correlation of H-160.

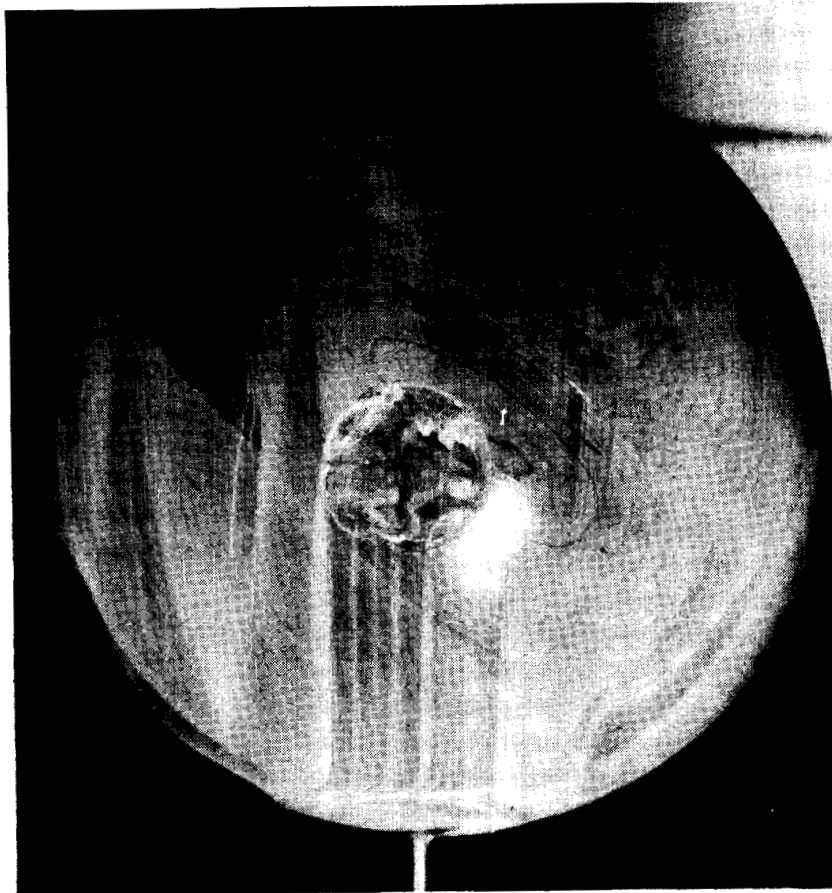
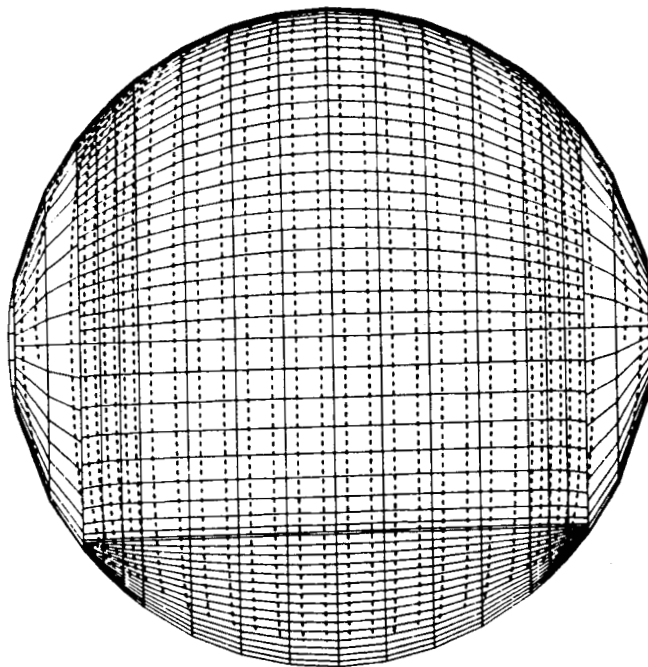


Figure 24.- Separation pattern on H-160 from oil flow visualization.



ORIGINAL PAGE IS  
OF POOR QUALITY

Figure 25.- Flow separation location predicted by VSAERO (H-160; planform view).

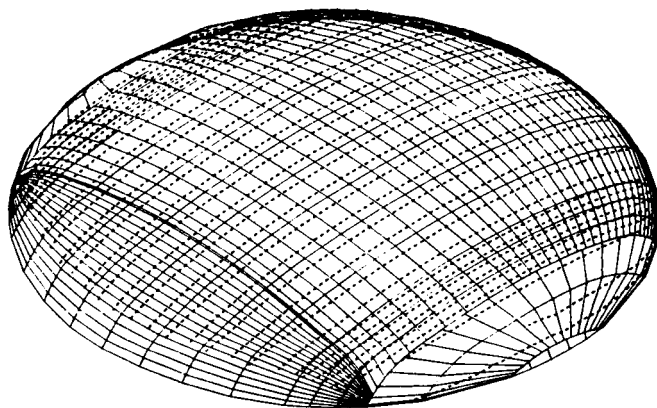


Figure 26.- Flow separation location predicted by VSAERO (H-160; oblique view).

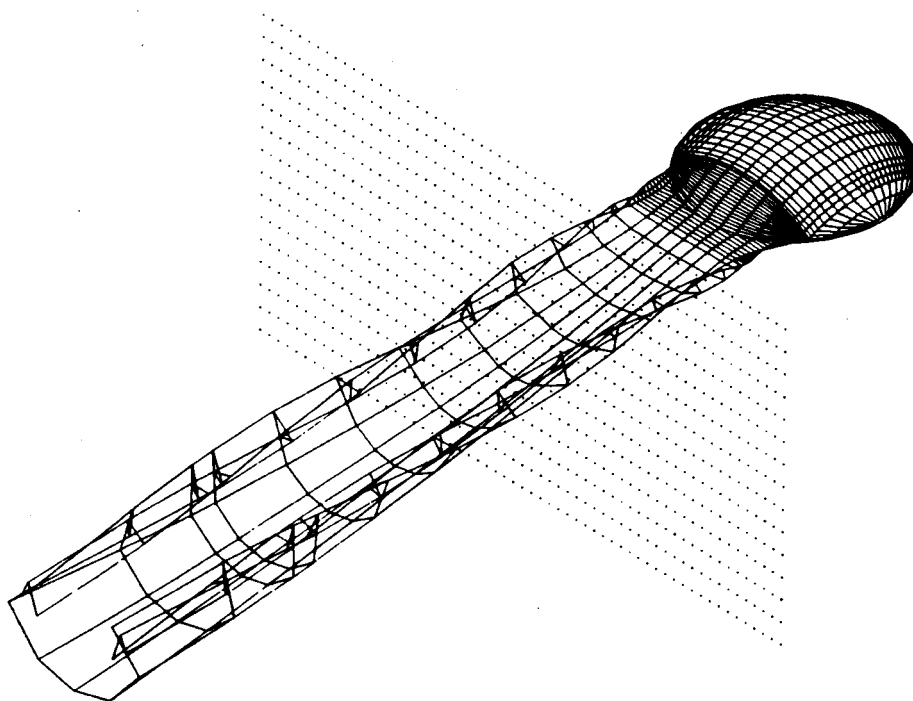


Figure 27.- Vortex sheet roll up simulated by VSAERO (H-50).

ORIGINAL PAGE IS  
OF POOR QUALITY

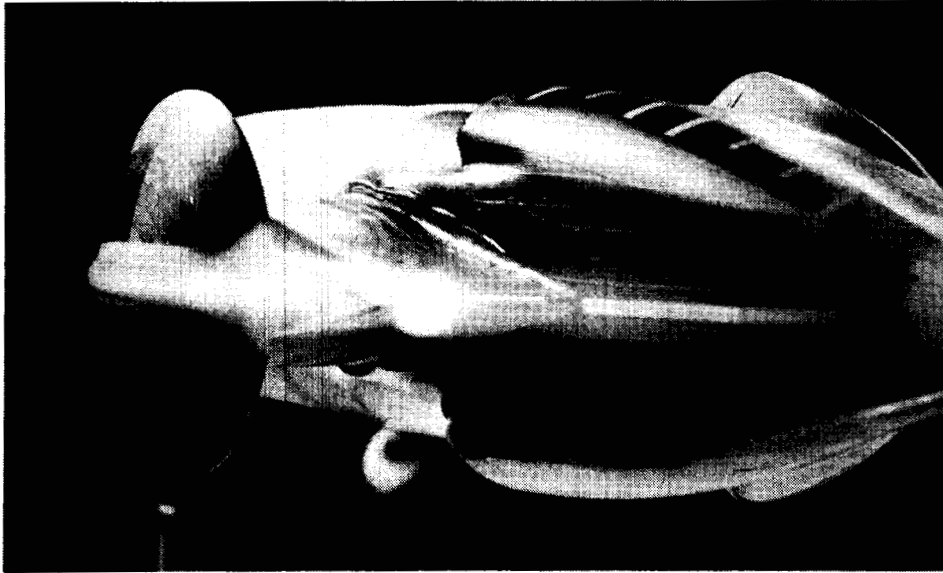
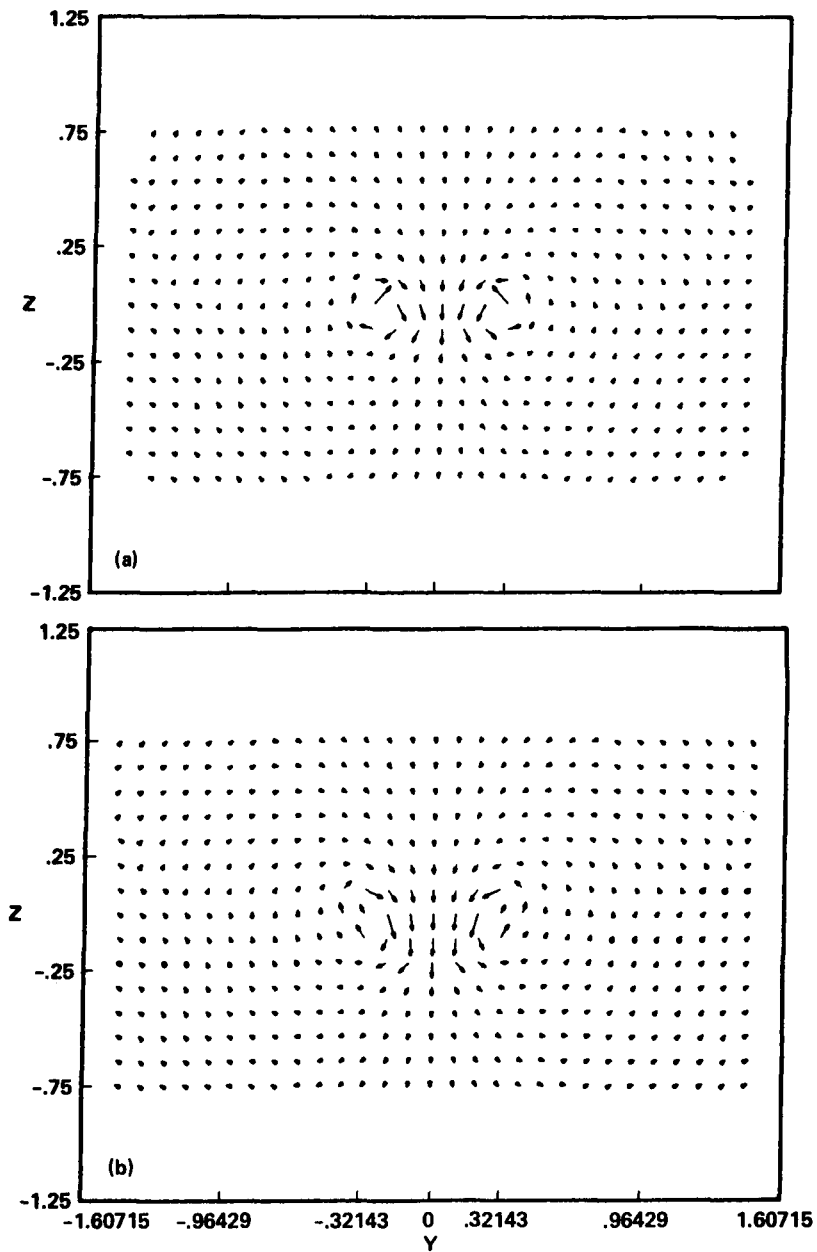


Figure 28.- Visualization of vortex roll up by laser sheet at  $1.02 D$  behind hub center (H-50).



Figure 29.- Visualization of vortex roll up by laser sheet at  $1.55 D$  behind hub center (H-50).



**Figure 30.- Visualization of vortex roll up with velocity vector plots generated by VSAERO. Planes at  $1.02 D$ (top) and  $1.55 D$  (bottom) behind hub center, viewing from downstream (H-50; isolated).**



# Report Documentation Page

<b>1. Report No.</b>  NASA TM-101048		<b>2. Government Accession No.</b>		<b>3. Recipient's Catalog No.</b>	
<b>4. Title and Subtitle</b>  Evaluation of VSAERO in Prediction of Aerodynamic Characteristics of Helicopter Hub Fairings				<b>5. Report Date</b>  February 1989	
				<b>6. Performing Organization Code</b>	
<b>7. Author(s)</b>  Alexander Louie				<b>8. Performing Organization Report No.</b>  A-88320	
				<b>10. Work Unit No.</b>  505-61-51	
<b>9. Performing Organization Name and Address</b>  Ames Research Center Moffett Field, CA 94035				<b>11. Contract or Grant No.</b>	
				<b>13. Type of Report and Period Covered</b>  Technical Memorandum	
<b>12. Sponsoring Agency Name and Address</b>  National Aeronautics and Space Administration Washington, DC 20546-0001				<b>14. Sponsoring Agency Code</b>	
				<b>15. Supplementary Notes</b>  Point of Contact: Alexander Louie, Ames Research Center, MS TR-031, Moffett Field, CA 94035 (415) 694-6976 or FTS 464-6976	
<b>16. Abstract</b>  A low-order panel code, VSAERO, was used to predict the aerodynamic characteristics of helicopter hub fairings. Since the simulation of this kind of bluff body by VSAERO was not documented before, the VSAERO solutions were correlated with experimental data to establish their validity. The validation process revealed that simulation of the aerodynamic environment around a hub fairing was sensitive to several modeling parameters. Some of these parameters are body and wake panels arrangement, streamwise and spanwise separation location, and the most prominent one—the wake modeling.  Three wake models were used: regular wake, separated wake, and jet model. The regular wake is a wake with negligible thickness (thin wake). It is represented by a single vortex sheet. The separated wake and the jet model in the present application are wakes with finite thickness (thick wake). They consist of a vortex sheet enclosing a region of low-energy flow. The results obtained with the regular wake were marginally acceptable for sharp-edged hub fairings. For all other cases under consideration, the jet model results correlated slightly better. The separated wake, which seemed to be the most appropriate model, caused the solution to diverge. While the regular wake was straight-forward to apply in simulations, the jet model was not. It requires the user to provide information about the doublet strength gradient on wake panels by guessing the efflux velocities at the wake shedding location. To obtain the correct doublet strength, these estimated velocities were matched to the calculated values. This involved an arduous and impracticable iterative process. In summary, VSAERO neither predicts accurately the aerodynamic characteristics of helicopter hub fairings nor was cost effective.					
<b>17. Key Words (Suggested by Author(s))</b>  VSAERO Hub fairings Wake models Aerodynamics characteristic			<b>18. Distribution Statement</b>  Unclassified-Unlimited  Subject Category - 02		
<b>19. Security Classif. (of this report)</b>  Unclassified		<b>20. Security Classif. (of this page)</b>  Unclassified		<b>21. No. of pages</b>  35	<b>22. Price</b>  A03